Simulation of Anisotropic Particle Shape Development during 2D Transformation†

M. C. Weinberg, D. P. Birnie, III,* and V. F. Farias

Department of Materials Science & Engineering, University of Arizona, Tucson, Arizona 85721

Received: March 29, 2002; In Final Form: June 3, 2002

Simulations were conducted of transformations involving anisotropic particles growing into a matrix of simultaneously growing isotropic particles. The ultimate shape development of the anisotropic particles, present in dilute concentration, was determined. The faster growing directions are found to impinge neighboring grains earlier in the transformation, thus creating a final particle morphology that is less eccentric than the shape would be if grown in isolation. The extent of this effect was determined as a function of intrinsic growth rate anisotropy and compared with analytical predictions.

Introduction

An extremely important, interesting, and challenging problem in transformation kinetics is elucidating the relationship between the shape of the transforming particles and the final morphology of the fully transformed material. There are two aspects to this problem. First, given information about the nucleation and growth rates of a particle and the particle shape, one would like to be able to predict the final morphology. However, a more difficult, but perhaps more useful, task is obtaining information regarding the transformation process and the particle anisotropy from knowledge of the final morphology.

In many instances, crystal growth occurs anisotropically (i.e., the crystal grows at different rates in different directions). Calculation of the kinetics of transformations involving anisotropic particles is a much more challenging problem than that for isotropic particles. The theory of the transformation kinetics for isotropic particles was developed by Johnson and Mehl,[1] Avrami,[2−4] and Kolmogorov[5] many years ago. The complicating features associated with transformation kinetics in which anisotropic particles are produced have been discussed previously.[6−11] As a consequence of these difficulties, there is a paucity of analytical theories describing such transformations. In most instances, computer modeling and simulations have been used instead.[6,12−16]

Ito and Fuller[15] have investigated the final morphologies in two-dimensional systems consisting of particles in the shapes of ellipses, octagons, hexagons, and triangles by simulation methods. They considered both the cases of pre-nucleation (site saturation) and continuous nucleation and growth. The authors showed results for grain size distributions, aspect ratio distributions, and the distribution of grains with different numbers of edges. The grain edge and grain size distributions were found to be quite insensitive to the shape of the particle. However, the aspect ratio distributions were somewhat dependent upon particle shape. Also, they observed a strong correlation between grain size distribution and distribution of grain edges, but little correlation was noted between the latter two distributions and the distribution of aspect ratios.

Nearly all of the computer simulation studies that have been performed were two-dimensional studies. However, several years ago Narayan[16] performed a computer modeling study of grain microstructure in three dimensions. Also, he described a programming scheme by which two-dimensional micrographs could be generated from the three-dimensional simulation results.

Despite the difficulties in describing the transformation kinetics of anisotropic particles, approximate and precise results have been obtained for several specific cases.[8,17−23] These studies have produced a qualitative understanding of the kinetics. Also, recently we have presented an analytical analysis of the development of anisotropic morphology due to growth of anisotropic particles in a matrix of growing isotropic particles in three dimensions.[24] It was assumed that the matrix particles followed ordinary JMAK kinetics. We described the change in anisotropic particle aspect ratio due to collisions with matrix particles. We analyzed such changes in particle morphology by computing the probabilities that certain growth rays of the anisotropic particle would encounter a growing matrix particle. The changes in particle morphology were studied as a function of the relative growth speeds of the anisotropic and matrix particles. In other related work, Roosen and Carter examined the growth and coarsening process with anisotropic growth rates using a simulation method.[25] Although their growth model is different than ours, they do monitor the growth anisotropy found in transforming and coarsening microstructures.

In the present work, we describe the results of a two-dimensional numerical simulation of a system similar to the one described above. We show grain edge distributions, aspect ratio distributions, and tilt angle distributions as a function of growth rate anisotropy. In addition, we present an analytical derivation for the final particle morphology in a two-dimensional system. The analytical results are compared with the numerical findings.

Model

In the present work, we consider the growth of a very dilute solution of anisotropic particles embedded in a matrix of growing isotropic particles. This model would represent the situation where two phases are growing simultaneously, one of which being symmetrical and the other asymmetrical. Also, it is required that the symmetrical phase be present in great excess. Here, we select the anisotropic particle to be ellipsoidal in shape, so that there is an axis of symmetry and only two characteristic

† Part of the special issue "John C. Tully Festschrift".

* To whom correspondence should be addressed. E-mail: Birnie@AML.arizona.edu.

10.1021/jp025859c CCC: $22.00
Published on Web 07/09/2002

growth speeds. The matrix particles are taken to be spherical. This situation can be satisfied experimentally if the overall composition is chosen appropriately. When the overall composition is such that its location in a binary phase diagram lies near that of the isotropic compound, only minor amounts of the anisotropic phase will form. We have selected this condition to be able to perform analytical calculations as well as computer simulations. If the anisotropic particles are present in appreciable concentration, then the problem becomes quite intractable due to the presence of blocking effects and phantoms.[6]

One may envision the growth behavior of the anisotropic particles by imagining the growth of a cluster of rays emanating from a point, and growing with a speed distribution characteristic of an ellipse. The growth speeds of the fast growth axis and the slow growth axis are denoted by v_a, v_b, respectively. One should note that for ellipsoidal particles, the fast and slow growth directions are spatially orthogonal. This feature allows one to select conditions such that possible interactions or coupling of the probabilities involved in growth of either of these perpendicular growth rays is prevented.

We assume that nucleation of both types of particles occurs prior to particle growth and is completed before the particles begin to grow. This assumption is an excellent representation of events in a two stage heating procedure used in experiments to measure nucleation rates in amorphous systems.[26−29] Also, we consider a 2-D system that is of infinite extent. The concentration of ellipsoidal particles is deemed sufficiently dilute so that anisotropic particle−particle interactions can be neglected. Particle growth is presumed to be interface controlled, so that all growth rates are constant. Also, the nucleation rate is assumed to be time independent.

Numerical Procedure

Computer simulations have been conducted that represent the physical processes described in detail above. We generate a field of randomly located neighboring particles, allow all the particles to grow (including the central particle that has elliptical growth habit), and monitor growth impingement between the central particle and any neighbors. After impingement, the final particle shape is analyzed in detail according to specific algorithms. Each of these stages of the calculation is described below in detail.

Field of Particles. The elliptical-growth-habit particle is placed at the origin of the coordinate system, which is defined so that the *X*-axis is pointed along the major axis of the ellipse. The "drand48" function[30] is used to generate pseudo-random (*X*,*Y*) locations from which circular-growth-habit particles will start growing, simultaneously. They are arbitrarily chosen to lie within a square that is centered at the origin. Early benchmarking of our program showed that even with a field of 200 matrix particles there were no randomly chosen configurations that resulted in unbounded growth. As a safety margin, we ran all simulations reported here with 400 particles. Reasonable statistics were acquired by running 25 000 random configurations.

Particle Growth and Determination of the Final Shape. Each particle in the system above is nucleated simultaneously. For the purposes of this description we will denote the growth rate assigned to the circular particles as "g". The elliptical particle is assigned growth rates v_x and v_y in the *X* and *Y* directions, respectively. At the outset we limit our simulations to cases where the minor axis growth rate is identical to the matrix growth rate. Thus, $g = v_y$ and $v_x \geq v_y$. We note that the choice of major axis is made without loss of generality since the distribution of circular particles about the origin is uniform. The growth rate of an elliptical growth ray $v_e(\theta)$ is given by

$$v_e(\theta) = \left[\frac{\cos^2(\theta)}{v_x^2} + \frac{\sin^2(\theta)}{v_y^2}\right]^{-1/2} \quad (1)$$

where, θ is the angle made by the growth ray with respect to the *X*-axis direction.

For the above growth law for the anisotropic particle, we examine how the various directions of growing rays interact with neighboring particles to determine the final morphology. When processing each nucleation pattern, we examine these rays at one-degree intervals so that the final shape of the resultant central particle is well represented. At locations where the nearest matrix particle changes index then the growth rays are examined at a much finer grid, as discussed below.

The calculations performed for each growth ray are the following: At a given angle θ we examine the intersection of the growth ray pointing in that direction with growth from all of the surrounding circular-growth-habit particles. We then determine the *earliest* intersection and this defines the coordinates of intersection required. The time of intersection with an elliptical particle growth ray growing at an angle θ with respect to the *x*-axis is given by the quadratic

$$(v^2 - g^2)t^2 - 2v(x_c \cos(\theta) + y_c \sin(\theta))t + (x_c^2 + y_c^2) = 0 \quad (2)$$

where (x_c,y_c) is the location of the center of the circular matrix particle, and other variables have been defined earlier. Clearly, the roots of this quadratic must have the same sign. If two negative roots arise, this indicates that the ray is growing away from the matrix particle and would never intersect it. Having two imaginary roots also indicates a condition where the ray does not intersect the particle. The condition where positive real roots arise indicates a possible intersection, with the smaller root being the candidate time. At a given θ, this process is repeated for every surrounding circular matrix particle and the earliest time of intersection is found. Knowing this time and the growth rate v(θ), we are then able to calculate the coordinates of intersection. The process is now repeated for every θ (with θ taking values from 0° to 359°) and hence a set of coordinates representing the final shape is obtained. Typically, only a small number of the matrix particles actually participate in bounding the central particle, even when several hundred particles are used to create the random crystallization field.

Nipped Corners. Depending on the resolution at which we examine growth rays, it is possible to *miss* intersections with some neighboring circular particles—though only ones that exhibit very tiny angular zones of intersection. These would be particles that would generate a grain face on the central particle that is extremely tiny and would fit between the grid selected above. To represent these graphically, we name them "nipped" corners because their addition amounts to nipping a very tiny corner from an *N* sided polygon to make one with $N + 1$ sides. If we do not account for these, then there could be some small amount of inaccuracy in the number of neighbors the central particle has. We tackle this problem in a very simple manner. At every three-grain junction identified (central particle plus two adjacent neighboring matrix particles), we examine the region between θ and $\theta + 1$ at every hundredth of a degree in a manner similar to the above. This largely eliminated the nipped corners problem, although there will be extremely rare occasions where a nipped corner would display an arc of smaller than 1/100°.

Grow Around. From eq 2, we note that at the boundary between conditions where there are two imaginary roots and conditions where there are real roots, we achieve the special case where both real roots are identical. This occurs at the point where a growth ray is almost fast enough to grow past a matrix particle and geometrically represents the case of the growth ray impinging orthogonally to a circular particle growth ray. This results in the condition of "grow around." To our knowledge, the anisotropic particle grow-around phenomenon has not been described in the literature, though the case of competing isotropic growth at different velocities has been well covered by Bradley and Strenski.[31] By careful examination of the root structure for eq 2, it can be shown that this can only occur for growth rays that are *faster* than the matrix particles. When grow around occurs, the imaginary-root-rays that are just adjacent to the grow around cusp will continue growing until they intersect with a second matrix particle—and this could be quite a bit further than the first matrix particle being avoided. Because the growth law described in eq 1 is strictly radial, then there will be a discontinuity in the locus of neighboring particle intersection points that generate the central particle's final shape. This discontinuity results from the choice of growth law. Matrix material could be more rapidly transformed if the growth law were designed to allow for transformations to continue around corners rather than proceed as straight rays. One example of such a growth law has been presented by Kobayashi et al.[32] In future work, we expect to examine the grow-around effect in greater detail to understand how important this might be for generalized transformation processes.

The method we use to identify locations of grow-around is quite simple. When it is determined that two adjacent rays (at the finer increment spacing) intersect different neighboring particles, we check to see that the neighbor identified at θ_i has a real intersection with the elliptical particle's growth ray at θ_{i+1} and vice-versa. If either of these condition is not satisfied, then we may safely conclude that for some θ in $[\theta_i,\theta_{i+1}]$, then the elliptical particle's growth ray is tangential to the locus of intersection with the circular particle under consideration, and grow around has occurred. Further analysis of the shadowed area available for grow-around transformation will be presented in a future paper.

Final Shape Ratio. We determine the "major axis" by calculating the inter-boundary-coordinate distances for all pairs of boundary coordinates and keeping track of the pair with the largest distance. For the purposes of this simulation the "minor axis" is defined as the length of the perpendicular bisector of the major axis. The ratio of the two gives us the final shape ratio. Note that the intersection point of the minor and major axes is not constrained to be at the origin where the anisotropic particle started its growth.

***XY* Shape Ratio.** For comparison with our earlier modeling work,[24] we calculate the ratio of growth length in the positive *X* and positive *Y* directions starting from the origin. Even though the growth in the *X* direction is known to be faster than that in the *Y* direction, the ray along the *X* direction could be shorter than the one in the *Y* direction due to an early collision with a matrix particle. So, if the ray growing toward $\theta = 0$ has length X_{inter} and the ray growing toward $\theta = \pi/2$ has length Y_{inter} then the *XY* shape ratio is defined to be the maximum of X_{inter}/Y_{inter} and Y_{inter}/X_{inter} and must always be a value larger than (or equal to) unity. This duality of choices allows one to assess the shape of the particle without needing knowledge about the intrinsic growth rates of the material in the two directions. Note that this metric *is* linked to the nucleation location.

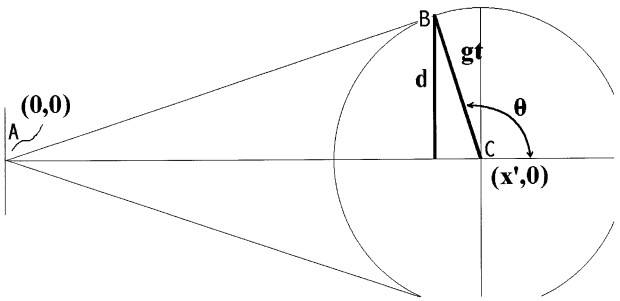

Figure 1. Illustration of the cumulative exclusion zone of a growing ray for time *t* when $v > g$. The cone area is made up of the superposition of all successively larger circles starting at (0,0) and extending to time *t*, when the ray has grown to $(x',0)$. Note that $x' = vt$.

Tilt Angle. This is defined as the angle made by the major axis with the *X*-axis, and is a direct outcome of the procedure used to find the major axis above.

These values have been measured for large numbers of randomly seeded fields of matrix particles in combination with a wide range of central particle anisotropies. The results of these simulations are presented below after we present an analytical treatment that corresponds to the metrics we gather from our simulations.

Analytical Method

Previously, we have performed a 3-D analysis to study the changes in particle morphology during the transformation process.[24] This examination was accomplished by deriving expressions for the probabilities that growth rays of the ellipsoid would travel a certain distance before encountering the growing matrix particles. A similar analysis is presented here for the 2-D case.

Consider a point $(x',0)$ in a plane that is not transformed at time t. It is assumed that this point is at the leading edge of a growth ray of an ellipse traveling along the positive *X*-axis. We denote the speed of this ray by v and the growth speed of all matrix particles by g. Because $(x',0)$ is not transformed at t, this fact indicates that there must be a circular region of radius gt around this point that does not contain matrix particle nucleation events. If this region had contained a matrix particle, then $(x',0)$ could not have been untransformed at time t. Furthermore, if the ray grows to $x' + v\Delta t$ in time Δt, then there is an exclusion circle of radius $g(t + \Delta t)$ around the point $(x' + v\Delta t,0)$. If Δt is small and $v > g$, then the two circles will overlap to a large extent, but some area of the second circle will lie outside of the first. To determine the conditional probability that the ray will go as far as $x' + v\Delta t$, given that it has reached vt, one must compute the area of the second circle that lies outside of the first.

To find the total probability that a ray will grow unimpeded until time t', one will have to construct a sequence of conditional probabilities of the type described above. If again, we consider only the case where $v > g$, then one will have a sequence of overlapping circles that will result in a geometric shape shown in Figure 1. Hence, to find the total probability that a ray grows for a time t, one must compute the area of this figure. It is clear from Figure 1 that 1/2 of this area is given as the sum of the area of the triangle ABC, A_Δ, and the partial circle, A_C, corresponding to an angle of rotation θ. It is clear that A_C is given by

$$A_C = \frac{1}{2}(gt)^2\theta \tag{3}$$

However, from Figure 1, it is clear that the triangle height of ABC can be used to evaluate θ and, hence, the partial circle area. Note that the complement to θ can be found using $\sin^{-1}(d/gt)$. Hence, eq 3 can be rewritten as

$$A_C = \frac{1}{2}(gt)^2\left[\pi - \sin^{-1}\left(\frac{d}{gt}\right)\right] \quad (4)$$

Also, from an inspection of Figure 1, it can be shown that d/gt can be expressed as $\{1 - (g/v)^2\}^{1/2}$, so finally we obtain

$$A_C = \frac{1}{2}(gt)^2\left[\pi - \sin^{-1}\left\{\left(1 - \left(\frac{g}{v}\right)^2\right)^{1/2}\right\}\right] \quad (5)$$

Clearly

$$A_\Delta = \frac{1}{2}dvt = \frac{vt}{2}(gt)\left(1 - \left(\frac{g}{v}\right)^2\right)^{1/2} \quad (6)$$

Therefore, we obtain for the total area, A_{tot}, the following expression

$$A_{Tot} = (gt)^2\left[\pi - \sin^{-1}\left\{\left(1 - \left(\frac{g}{v}\right)^2\right)^{1/2}\right\} + \frac{v}{g}\left(1 - \left(\frac{g}{v}\right)^2\right)^{1/2}\right] \quad (7)$$

Thus, if ρ is the number density of isotropic particles, then the probability that a ray grows for a time t, $Z(t)$, is given by eq 8

$$Z(t) = \exp\left\{-\rho(gt)^2\left[\pi - \sin^{-1}\left\{\left(1 - \left(\frac{1}{w}\right)^2\right)^{1/2}\right\} + w\left(1 - \left(\frac{1}{w}\right)^2\right)^{1/2}\right]\right\} \quad (8)$$

In eq 8, w is the ratio of the speed of the ray to the growth rate of the isotropic particle ($w = v/g$). Because a ray will grow a distance $x = vt$ in a time t, and if we denote the quantity in square brackets in eq 8 as $\phi(w)$, then the probability that a ray will grow a distance x is as follows

$$Z(x) = \exp\left\{-\left[\Phi(w)\frac{\rho}{w^2}\right]x^2\right\} = \exp(-\beta x^2) \quad (9)$$

with β being defined by the quantity in square brackets in eq 9. If $P(x)$ is the probability density that a ray reaches some length between x and $x + dx$, then

$$P(x) = -\frac{dZ}{dx} = 2\beta x \exp(-\beta x^2) \quad (10)$$

Now we consider two orthogonal rays from the same anisotropic particle traveling in the positive directions (i.e., the fast and slow growth directions, major and minor axes of the ellipse). We are interested in computing the expected ratio of the lengths of these two rays because the change in this quantity from its ideal value of v_a/v_b will provide a measure of the distortion of particle shape due to collisions with matrix particles.

For the following analysis, we assume that the growth of these two orthogonal rays occurs independently. Geometric conditions that satisfy this assumption were derived in our previous analysis for 3D growth.[24] If we let r be the ratio of the ray lengths along the two axes, then we have shown in ref 24 that the total probability that r does not exceed some specific value r^* is given by eqs 11a−c

$$P_{tot} = P_+ + P \quad (11a)$$

$$P_+ = \int_1^{r^*}\frac{dr}{r^2}\int_0^{x_{a,max}} x_1 P_a(x_1) P_b\left(\frac{x_1}{r}\right)dx_1 \quad (11b)$$

$$P_- = \int_1^{r^*}\frac{dr}{r^2}\int_0^{x_{b,max}} x_2 P_a\left(\frac{x_2}{r}\right) P_b(x_2)dx_2 \quad (11c)$$

In eq 11b,c, $x_{a,max}$ and $x_{b,max}$ are the maximum possible extensions of the rays along the x_1 and x_2 axes at time t, respectively (i.e., assuming they had not collided with matrix particles). Also, P_a, P_b are given by eq 10 with a and b referring to rays along the fast and slow growth axe directions. The term $P_b(x_1/r)$ is the probability density that the Y-directed ray grows to length $x = x_1/r$, and $P_a(x_2/r)$ is the probability density that the X-directed ray grows to length $x = x_2/r$. Both of these distances are required to establish r at specific relevant values during integration. The term described in eq 11c then describes the contribution to final shape that occurs when the faster growth ray is blocked by a matrix particle at a shorter distance than the slower growing ray.

Because the probability density of finding a length ratio between r^* and $r^* + dr^*$, P^d, is given by the derivative of P_{tot} with respect to r^*, one finds

$$P^d = P_+^d + P_-^d = \frac{1}{(r^*)^2}\left\{\int_0^\infty x_1 P_a(x_1) P_b\left(\frac{x_1}{r}\right)dx_1 + \int_0^\infty x_2 P_a\left(\frac{x_2}{r}\right) P_b(x_2)dx_2\right\} \quad (12)$$

If one defines $s = \beta_b/\beta_a$, then the following results are obtained

$$P_+^d = \frac{2r^*s}{[(r^*)^2 + s]^2} \quad (13a)$$

$$P_-^d = \frac{2r^*s}{[s(r^*)^2 + 1]^2} \quad (13b)$$

A quantity of particular interest is the average value of r^* because this quantity serves as a measure of the alteration in particle shape caused by collisions with growing isotropic particles. If the average value of r^* is denoted by $\langle r^*\rangle$, then

$$\langle r^*\rangle = \int_1^\infty r^* P^d(r^*)dr^* \quad (14)$$

If one employs eqs 13a,b in eq 14, then the average length ratio is given by the expression in eq 15

$$\langle r^*\rangle = 1 + \sqrt{s}\left(\frac{\pi}{2} - \tan^{-1}\left(\frac{1}{\sqrt{s}}\right)\right) + \frac{1}{\sqrt{s}}\left(\frac{\pi}{2} - \tan^{-1}(\sqrt{s})\right) \quad (15)$$

eq 15 will be employed in a subsequent section to compute $\langle r^*\rangle$ analytically and the results of such calculations will be compared with our computer simulations. This term compares directly with the "*XY*-shape ratio" morphology metric described above.

Results and Discussion

Simulation runs have been carried out for elliptical particles having different inherent anisotropy of growth habit. We designate this inherent anisotropy of particle growth as the "Growth Rate Anisotropy" or GRA, and we define it as the major axis to minor axis ratio for the growth law defined above. In other words, GRA $= v_x/v_y$ and is always greater than or equal to unity. In all the simulations that we report here, we have

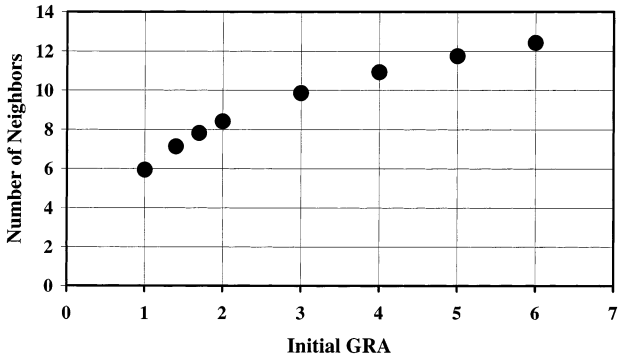

Figure 2. Average number of sides for elliptical grains having various levels of intrinsic growth rate anisotropy (GRA). GRA values start at one for perfectly spherical growth.

selected the matrix growth rate to be equal to the minor axis growth rate for the elliptical particle, but this need not be true in the general case.

Number of Neighbors. One basic metric observed in the simulations was the number of neighboring matrix grains that the central particle impacted during its growth for each starting condition. Figure 2 plots the average number of neighbors as a function of GRA and illustrates a general increase as major axis growth velocity increases. These data are directly consistent with the growth process we are modeling. For GRA = 1 the central particle is growing in a manner identical to that of the matrix particles. Under such conditions the ideal average number of neighbors is exactly 6.[33,34] Conducting multiple runs of 5000 configurations we have found that our average value is 5.95 ± 0.01.

As the GRA gets larger, then we find that there are more neighbors, as one would expect, though the increase is less dramatic at larger GRA. If the final particle shape were well represented by an ellipse having an aspect ratio identical to the starting GRA, then we might expect that the final number of neighbors would scale with the perimeter of the eccentric ellipse. The perimeter of an ellipse having minor axis with a length of unity and a major axis with a length of w is given by eq 16

$$\text{Perimeter} = \pi\left[\frac{3}{2}(w+1) - \sqrt{w}\right] \qquad (16)$$

So, for circular growth ($w = 1$) we find a perimeter of 2π (giving an ideal neighbor count of 6). If the number of neighbors scaled linearly with the expected particle perimeter then we would expect something more than 24 neighbors when the central particle has GRA = 6, yet the simulations show that such conditions result in an average neighbor count around 12.4 (see Figure 2). So, a simple connection to the intrinsic elliptical shape is not found.

The number of neighbors may be more directly influenced by the random placement of matrix particles around the central particle. In other words, the neighbor count may start to saturate simply due to the fact that nearby matrix particles may block the growth before it can grow out to its full ideal elliptical shape. Certainly, the faster growing directions are able to outpace some of the nearby matrix particles thus resulting in a greater neighbor count. However, the derivation given above in eq 15 has shown that the final particle shape will not grow linearly with the starting anisotropy. So, we might expect a more gradual increase in neighbor count along with the particle blunting effect.

Final Particle Orientation. The next simple measurement of the resultant microstructures is the distribution of final particle orientations. This is important to quantify because the statistical

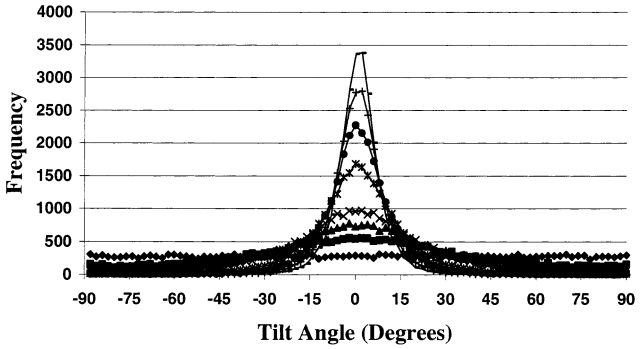

Figure 3. Distribution of apparent particle orientation as determined by finding particle major-axis lines from the final particle morphology. The tilt angle is measured in degrees and is referenced to the *X*-axis direction. For GRA = 1, we have no directional growth preference so all orientations are equally probable. Anisotropic particles are preferentially aligned with respect to the growth major-axis. GRA values of 1.0, 1.4, 1.7, 2, 3, 4, 5, and 6 are presented and exhibit gradually stronger preferred orientation.

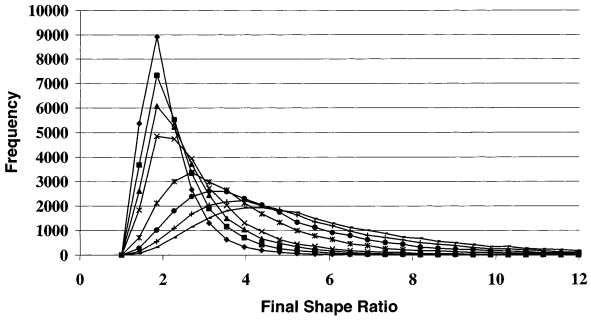

Figure 4. Distribution of Final Shape Ratio for several values of intrinsic growth rate anisotropy (GRA). GRA values of 1.0, 1.4, 1.7, 2, 3, 4, 5, and 6 are presented and cause the peak to shift toward the right, representing more elongation.

distribution of the neighboring matrix particles provides the environment within which growth occurs. Sometimes matrix particles will be situated close to the fast growth directions and so such rays will only grow for very short times before impinging a matrix particle. Therefore, the *apparent* major axis can easily be tilted away from the fast growth direction as a result of these interactions. Typically, microstructure analysis of transformation structures occurs after the-transformation is completed. The variance between true fast-growth-direction and final particle shape is very interesting and is given in Figure 3. The distribution shows strong preference for alignment near the major axis for particles that exhibit growth anisotropy. The distribution is still quite broad around that fastest growth direction. We believe that this is due to the statistical effect of the field of randomly located neighboring particles.

Final Particle Shape. As described in an earlier section, we have quantified the final particle shape in two distinct ways. First, we have done a shape analysis of the final particle morphology that results from impingement with neighboring matrix particles. Second, we have examined the resultant growth distances in the *X*- and *Y*-axis directions and compared these numbers with those predicted by our analytical derivation. As noted above, the major-axis of the final particle morphology is not required to be aligned with the starting particle's growth habit. Instead, it is defined by a combination of neighbor locations and growth velocity competition effects.

Figure 4 shows the distribution of "Final Shape Ratio" of the central particle's morphology, based on finding the chord connecting vertexes and measuring the midpoint perpendicular

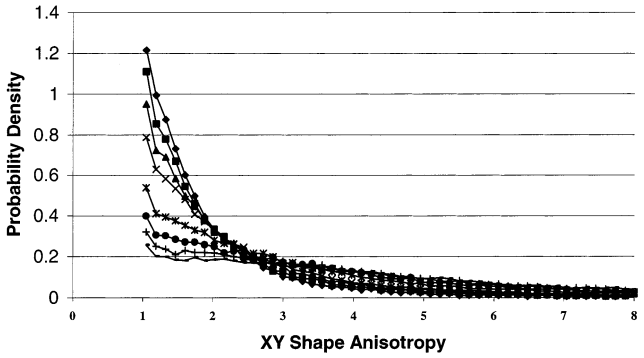

Figure 5. Distribution of Final *XY* Shape Ratio for several values of intrinsic growth rate anisotropy (GRA). This plots the ratio of the growth in major axis and minor axis directions (aligned with the *X* and *Y* axes of the coordinate system).

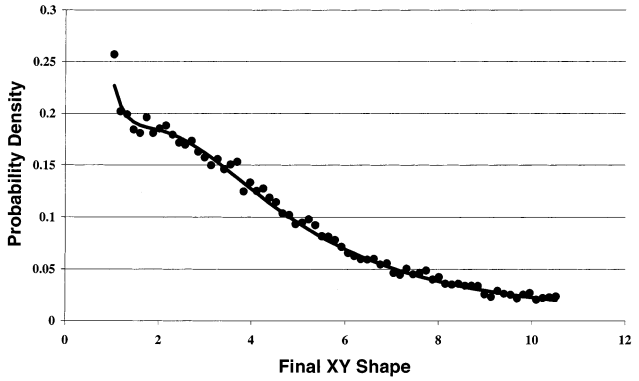

Figure 6. Distribution of Final *XY* Shape Ratio comparing the analytical result (solid line) from eqs 12 and 13 and the simulation (circles). These data are for GRA = 6.

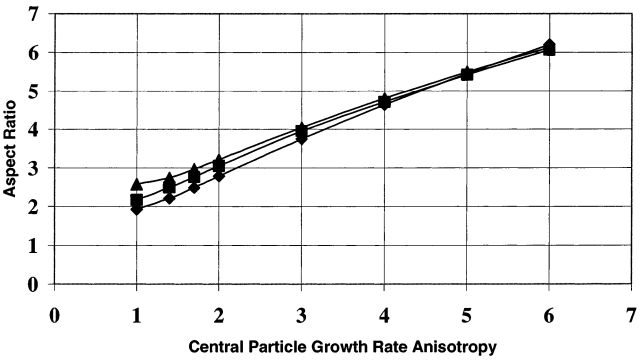

Figure 7. Weighted averages for final aspect ratios according to the two key metrics used in this paper. Diamonds are the "Final Aspect Ratio," which had the distribution presented above in Figure 4. Squares are for the "Final *XY* Shape Ratio," which had the distribution presented above in Figure 5. Triangles are calculated results for the analytical model and compare directly with the Final *XY* Shape Ratio data, as discussed fully in the text.

width for comparison. This is equivalent to shape analyses that are often performed in automated microstructure analysis software packages. One especially interesting feature of these distributions is that particles with small GRA (nearly circular growth) still evolve into particles that have distinct anisotropy on average. This is a direct result of the growth process into a field of randomly located particles that define the ultimate shape of each central particle. In other words, the longest chord of the resultant particle will likely exist where gaps between neighboring particles exist on nearly opposite sides of the nucleation location of the test particle. The peak in the distribution shifts toward larger anisotropy as the growth law gets more elliptical, but the shift is more gradual than the change in growth rate in that direction. Note that the GRA = 1 data peak at around 1.5, whereas the GRA = 6 data peak at around 3.5 or so. The final weighted average particle aspect ratio will be presented below after showing the distribution of our other shape metric.

Figure 5 shows the distribution in aspect ratios determined from analysis of the final particle shapes found in our simulations. Again, the more circular particles have their distribution concentrated at the left of the figure. As more elliptical particles are used, then the distribution broadens toward higher ratios. As noted before, this ratio allows for the possibility that the faster growth ray (moving along $+X$) might impinge on a neighboring particle closer to the origin than the slower growing ray (moving along $+Y$). This collision time comparison is again controlled by the statistical distribution of locations of matrix particles in each combination being tested. The ratio is defined in these terms to be consistent with our analytical derivation presented above (and derived before for 3D systems[24]). It is interesting to note that the probability distributions found from our simulations are an excellent match to the prediction given in eqs 13 above. Figure 6 shows a comparison between the simulation and analytical predictions.

Figure 7 presents the average particle aspect ratios according to the two above metrics along with our analytically derived result. The average "Final Shape Ratio" and the average "Final *XY* Shape" are presented for increasing values of GRA for the central particle. Note that even for GRA = 1, the central particle will have some net anisotropy in the final analysis. This occurs as a result of the random locations where matrix particles are found in the areas nearby the origin. The values for these two metrics are quite similar, though the *XY* axis ratio is a little bit larger than the "Final Shape Ratio". This is due to the fact that the *XY* measurement is controlled by the placement of the nearest two particles along *X* and *Y* axis directions, while the final morphology (and thus the final aspect ratio) of the whole particle is defined by numerous surrounding particles (typically averaging at least 6, depending on GRA).

It is interesting to compare our results with an earlier simulation of anisotropic particle transformations performed by Ito and Fuller.[15] For some of their calculations, they used an elliptical growth law identical to ours, but their simulation allowed all particles to transform with this identical law. In their work, they define the ellipse aspect ratio inversely to our definition, but have presented histograms of final particle morphology measured from the resultant 2D microstructures. They performed simulations with shapes equivalent to GRA = 1, 2, and 3.3333. By carefully analyzing their particle shape histograms we estimate that their average particle shapes for these conditions are about: 1.6, 1.9, and 2.3, respectively. Their values appear to be somewhat smaller than the corresponding values from our simulations: 1.93, 2.78, and ~4 (by interpolation). We believe that part of this difference is due to the difference in how we measure the aspect ratio. Their aspect ratio definition is forced to have the major and minor axes pass through the nucleation site. However, most microstructural analysis procedures perform this analysis independent of this knowledge—as our procedures described above. This freedom to pick the longest chord through the final particle will tend to shift the average value up for each particle analyzed. Therefore, we believe that our numbers are in substantial agreement with the Ito and Fuller data.

The work of Roosen and Carter also provides some interesting comparison for this growth anisotropy process.[25] In their work,

they looked at the nucleation and growth (and ultimate coarsening) of particles in a matrix supersaturated in the constituent that was crystallizing. Although they simulate particles with an inherent growth anisotropy of 20, the peak anisotropy shown in their figures reaches only about a factor of 1.7; we interpret their aspect ratio quantity to be equivalent to a GRA of about 3 in our definition framework. This anisotropy peak appears to have occurred at times that are relatively short, before growth had reached its saturation point. It is possible that depletion of the supersaturation field around the growing particles has kept them from exhibiting the anisotropy that they would otherwise show (base on the defined intrinsic boundary mobilities).

The variations and trends exhibited in Figure 6 are illustrative of the processes that control final morphology during microstructure development. Two key factors play important roles: inherent growth anisotropy and the statistical placement of neighboring particles. At very low GRA (inherent growth anisotropy) the aspect ratio is controlled by the locations of the neighboring particles. Thus, even at GRA = 1 (a completely isotropic central particle) the final morphology is expected to be around 2, whether the "Final Shape Ratio" or "Final *XY* Shape" criterion is used. Typically, the random nature of matrix particle formation will allow certain rays to grow further than others prior to encountering a growing isotropic particle, thus resulting in anisotropic final shapes.

At larger values of GRA the final aspect ratio of the particle is also larger. The situations found at larger GRA define conditions that will be more strongly controlled by the growth velocity competition rather than the random placement of particles in the near field. This feature of the large GRA interactions is demonstrated by the fact that the analytical results show close overlap with the simulation results at larger GRA (see Figure 7). Using eq 15 at even larger GRA values allows us to recognize that the expected *XY* shape will scale approximately as the square root of GRA, though this behavior becomes more apparent at GRA values of 10 or more. For example, the expected *XY* shape at GRA = 10 is about 8.2, but the expected *XY* shape at GRA = 100 is only about 28, an increase by about a factor of 3.4 or so. This is consistent with the trends displayed by particle morphology in 3D.[24]

It is interesting that the analytical result in eq 15 deviates somewhat from the simulation results at low GRA value. The average *XY* aspect ratios measured in the simulations are consistently lower than the value determined from eq 15. This is thought to be a result of the fact that the assumption of independent growth along *X* and *Y* directions is not strictly maintained in reality. The result of this breakdown is that there will be some situations found in simulations where a *single* matrix particle will be located where it can block the growth of *both X* and *Y* directed growth rays. These occurrences are more likely with *XY* shapes that are close to unity, thus biasing the final result toward the smaller side. In fact, by choosing to have the minor axis growth rate be identical with the matrix particles' growth rate for the present simulations may have made the independence assumption overly weak. Future work will attempt to map out this part of the parameter space. In our 3-D derivation presented earlier,[24] we analyzed this limit and found that the minor axis growth rate must be $\sqrt{2}$ times faster than the matrix particles to avoid this kind of interaction.

Grow Around Frequency. As noted above in the numerical procedure section, there are some situations where the direct radial growth law that we have chosen may give discontinuities in the final particle morphology. These present locations where the faster growing ray from the central particle would be able to grow around into untransformed area behind the growing neighboring particle. Figure 8 shows how often three-grain-junctions around the central particle's perimeter have discontinuities where grow-around would occur. When the central particle grows in a manner that is identical to the matrix particles then no grow around can ever occur (cf., GRA = 1 data in Figure 8). However, when central particle growth rays are growing faster than the matrix particle then grow around can occur. Note that the frequency of grow-around climbs rather rapidly. Comparing the numbers in Figure 8 with the final neighbor counts shown in Figure 2, we can see that even at GRA = 4 about half of the grain intersections around the perimeter will be places where grow around can occur. At larger GRA, the effect is even more pronounced. This highlights a geometric limitation of the directly radial elliptical growth law that we (and others) have used. When elliptical particles are growing into a matrix of elliptical particles, then there are some configurations where the random placement of anisotropic particles will not be able to convert all locations within the coordinate space. This is the first time that this geometric limitation has been reported, despite several previous studies involving elliptical or ellipsoidal particles.[6,12−15] The actual area that could be transformed through these grow-around gaps has not been evaluated in the present study since this requires a new growth law, which is beyond the scope of the present work. We note that Kobayashi et al.[32] have used a mean-field approach to cover this case, but the grow around effect seems to be rather small unless the growth anisotropy is very large. This is in contrast to the indications that we found above showing that the frequency of grow around locations is rather high. These findings may be compatible, but significant further work on the grow around phenomenon is still warranted.

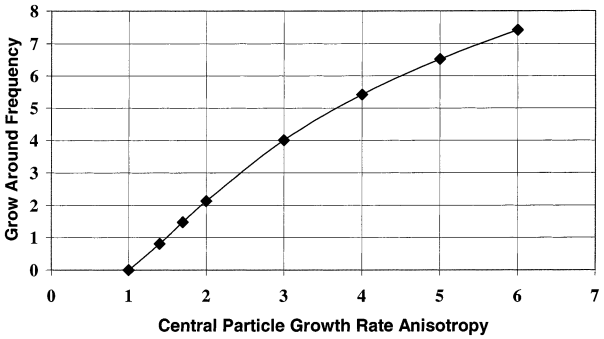

Figure 8. Average frequency of grow-around as a function of central particle growth rate anisotropy (GRA). These numbers should be compared with average number of neighbors found in the final particle morphology.

Summary. The simulations and analytical results presented here have shown a number of interesting effects for anisotropic particle growth in phase transformations. Our results are based on the reduced growth time allowed for growth rays that are traveling faster than the matrix particles are growing (geometrically assessed using Figure 1). We noticed these features of the anisotropic transformations:

- Because faster rays are stopped at relatively shorter times, the final grain morphology is blunted with respect to the particles inherent growth law.
- The inherent growth anisotropy *and* random placement of neighboring particle both contribute to the apparent anisotropy seen in real microstructures.
- For the first time, we have quantified the "grow around" effect and how it depends on growth velocity relative to the matrix growth rate.

• Finally, we have verified our probabilistic derivation of expected growth distance and expected *XY*-shape, especially at large growth anisotropy where orthogonal directions grow independent of one another.

Conclusions

Computer simulations have been compared with analytical derivations of final particle morphology that results when both isotropic and anisotropic particles simultaneously participate in phase transformations in two dimensions. The final particle morphology is determined by two broad factors: the inherent particle growth rate anisotropy as well as the statistical placement of neighboring particles in the near field. The particle's growth anisotropy exerts a greater control when its rapidly growing rays are much faster than that of the matrix particles. On the other hand, the random placement of neighboring particles is more important for less eccentric central particles.

Acknowledgment. We extend our great appreciation to Dr. S. Slovin for her support to one of us (M.C.W.).

References and Notes

(1) Johnson, W. A.; Mehl, R. *Trans. AIME* **1939**, *135*, 416.
(2) Avrami, M. *J. Chem. Phys.* **1939**, *7*, 1103.
(3) Avrami, M. *J. Chem. Phys.* **1940**, *8*, 212.
(4) Avrami, M. *J. Chem. Phys.* **1941**, *9*, 177.
(5) Kolmogorov, A. N. *Izv. Akad. Nauk SSR, Ser. Fiz.* **1937**, *3*, 355.
(6) Shepilov, M. P.; Baik, D. S. *J. Non − Cryst. Solids* **1994**, *171*, 141.
(7) Starink, M. J. *J. Mater. Sci.* **2001**, *36*, 4433.
(8) Weinberg, M. C.; Birnie, D. P., III. *J. Non-Cryst. Solids* **1995**, *189*, 161.
(9) Shepilov, M. P. *Sov. Phys. Crystallogr.* **1990**, *35*, 164.
(10) Weinberg, M. C. *J. Non-Cryst. Solids* **1999**, *255*, 1.
(11) Bianchet, M. A.; Rigotti, G.; Blesa, M. A. *Solid State Ionics* **1990**, *42*, 21.
(12) Pusztai, T.; Granasy, L. *Phys. Rev. B* **1998**, *B57*, 14110.
(13) Kunaver, U.; Kolar, D. *Acta Mater.* **1998**, *46*, 4629.
(14) Kolar, D.; Kunaver, U.; Recnik, A. *Phys. Status. Solidi A* **1998**, *166*, 219.
(15) Ito, O.; Fuller, E. R., Jr. *Acta Metal. Mater.* **1993**, *41*, 191.
(16) Narayan, K. L. *Comput. Phys. Commun.* **1996**, *93*, 136.
(17) Birnie, D. P., III.; Weinberg, M. C. *J. Chem. Phys.* **1995**, *103*, 3742.
(18) Weinberg, M. C.; Birnie, D. P., III. *J. Non-Cryst. Solids* **1996**, *196*, 334.
(19) Birnie, D. P., III.; Weinberg, M. C. *Physica A* **1996**, *223*, 337.
(20) Birnie, D. P., III.; Weinberg, M. C. *Scripta Mater.* **1996**, *35*, 361.
(21) Weinberg, M. C.; Birnie, D. P., III. *J. Chem. Phys.* **1996**, *105*, 5138.
(22) Birnie, D. P., III.; Weinberg, M. C. *Physica* **1996**, *A230*, 484.
(23) Weinberg, M. C.; Birnie, D. P., III. *J. Non-Cryst. Solids* **1996**, *202*, 290.
(24) Birnie, D. P., III.; Weinberg, M. C. *Physica A* **2000**, *285*, 279.
(25) Roosen, A. R.; Carter, W. C. *Physica A* **1998**, *261*, 232.
(26) Burgner, L. L.; Weinberg, M. C. *J. Non-Cryst. Solids* **2000**, *216*, 163.
(27) Ramesh, R.; Nestor, E.; Pomeroy, M. J.; Hampshire, S.; Liddell, K.; Thompson, D. P. *J. Non-Cryst. Solids* **1996**, *196*, 320.
(28) Arita, I. H.; Wilkinson, D. S.; Purdy, G. R. *J. Am. Ceram. Soc.* **1992**, *75*, 3315.
(29) Davis, M. J. *J. Am. Ceram. Soc.* **2001**, *84*, 492.
(30) The "drand48" function generates pseudorandom number within the interval [0.0, 1.0] using a linear congruential algorithm for successive number generation. See, The Single UNIX® Specification, Version 2, Copyright © 1997, The Open Group.
(31) Bradley, R. M.; Strenski, P. N. *Phys. Rev. B* **1989**, *B40*, 8967.
(32) Kobayashi, R, Warren, J. A., Carter, W. C. *Physica D* **1998**, *D119*, 415.
(33) Iglesias, J. R.; de Almeida, R. M. C. *Phys. Rev. A* **1991**, *43*, 2763.
(34) Moore, R. E. M.; Angell, I. O. *J. Comput. Phys.* **1993**, *105*, 301 − and references therein.